A Long-Term Overshooting Convective Cloud Top Detection Database Over Australia Derived From MTSAT Japanese Advanced Meteorological Imager Infrared Observations

Kristopher M. Bedka
Science Directorate
NASA Langley Research Center
21 Langley Boulevard, Mail Stop 420, Hampton, VA 23681 USA

John T. Allen
International Research Institute for Climate and Society,
The Earth Institute of Columbia University, Lamont Campus
61 Route 9W, Palisades, New York 10964 USA

Submitted For Publication In
Geophysical Research Letters

May 30, 2016

Three Key Points

1) Hazardous storms often have one or more overshooting cloud tops that indicate strong updraft regions are detectable within geostationary satellite imagery

2) An automated overshooting cloud top (OT) detection method has been applied to a 10-year data record of MTSAT JAMI imagery

3) The OT database showed three distinct regional maxima, differences in storm activity between land and ocean, and the impact of topography on storm distribution

ABSTRACT

Geostationary (GEO) satellite imagers have been collecting spatially- and temporally-detailed observations of deep convection for over 20 years, providing useful insight into the development and evolution of hazardous storms. Hazardous storms often produce one or more overshooting cloud tops (OT) that indicate the location of strong updrafts where weather hazards are typically concentrated. Long-term GEO data records can be processed within an automated OT detection algorithm to characterize the climatological distribution of hazardous storms. GEO OT databases are especially valuable in regions without ground-based radar or lightning sensor networks and for analyzing the diurnal cycle of hazardous storms, complementing analyzes derived from polar- or low-inclination-orbiting satellite instruments. In this paper, we describe a 10-year GEO OT detection database over Australia that highlights regional variability and sharp differences in storm activity between land and ocean across the diurnal cycle.

Introduction and Background

Geostationary (GEO) satellite imagers provide routine observations of deep convection across the much of the globe. GEO imager observations are critical to the weather forecasting community for identifying when and where storms are likely to develop, determining storm movement, and estimating storm severity especially over regions without ground-based weather radar or lightning detection network coverage. Hazards such as damaging wind, hail, tornadoes, lightning, and heavy rainfall are typically concentrated near intense updrafts that can penetrate through the local equilibrium level and produce a signature often referred to as an overshooting cloud top (OT, Bedka et al. 2010; Dworak et al. 2012 and references therein). GEO images collected at 1-minute resolution show that OTs typically exist for only a few minutes, but some OTs in especially hazardous and long-lived storms such as supercells can persist for longer than 30 mins [Bedka et al. 2015].

Given the rapidly evolving nature of hazardous storms and day-to-day differences in storm coverage, it can be difficult for the weather forecasting and climate analysis communities to understand where and when these storms occur most frequently. Previous studies have shown that an automated GEO-based OT detection method applied to a consistent long-term satellite infrared (IR) brightness temperature (BT) data record can be used to produce high-quality and spatially detailed hazardous storm distributions [Bedka et al. 2010 (B2010 hereafter); Bedka 2011; Proud 2014; Thiery et al. 2016]. Two illustrations of using the B2010 OT detection product for climate analysis are identification of a distinct OT maximum associated with intense nocturnal thunderstorms over each of the African Great Lakes [Thiery et al 2016], and a nine-year European OT detection database combined with ground-based reports of hail and numerical weather prediction model data to develop the first pan-European hail risk model [Punge et al. 2014].

The Australia region is similar to Europe and the Lake Victoria region in that a long-term, climate-quality, and spatially contiguous radar data network does not exist. This requires researchers to use other ground-based, reanalysis proxy, and space-borne datasets to define the climatological behavior of hazardous storms. Ground-based observations of thunderstorms at weather reporting stations have been used to construct a 10-year map the number of days with thunder [Kuleshov 2012]. Relative maxima in thunder-days were located across the Northern Territory (NT), northern Queensland (QLD), the eastern edge of Western Australia (WA), and along the southeastern coast of the continent. Lightning flash density derived from ground-based detection networks generally agrees with the thunder-day distribution [Kuleshov 2012; Virts et al. 2013, Dowdy and Kuleshov 2014]. Recent efforts have also been made to explore the occurrence of these storms using hail and tornado observations [Allen and Allen 2016], and environments favorable to the development of such storms as a proxy [Allen et al. 2011; Allen and Karoly 2014]. These studies have revealed that severe thunderstorms predominantly occur south of the tropical latitudes, and are found most often over the east of the continent but also occur over interior WA.

Space-borne instruments used to characterize regional storm distribution and temporal evolution over Australia consist of optical lightning detection sensors, passive microwave imagers, precipitation radar, and passive GEO IR imagers. Data from the Optical Transient Detector (OTD) on the MicroLab-1 satellite and the Lightning Imaging Sensor (LIS) on the Tropical Rainfall Measuring Mission (TRMM) satellite, have been used to construct a lightning climatology of diurnal behavior and interannual variability in flash rates from 1995-2010 across much of the globe including Australia and offshore waters, augmenting lightning distributions derived from ground-based lightning sensors [Kuleshov 2012; Cecil et al. 2014; Cecil et al. 2015]. Passive microwave brightness temperature (BT) observations from polar-orbiting instruments such as the Advanced Microwave Scanning Radiometer for Earth Observing System (AMSR-E) and the Advanced Microwave Sounding Unit (AMSU) have also been used to identify strong convection and serve as a proxy for severe hail events [Cecil and Blankenship 2012; Ferraro et al. 2014]. These proxies identified hail events along the northern and eastern coasts of the continent, though few ground observations of hail are recorded in northern Australia, and the approach over-detects hail in tropical regions [Allen and Allen 2016]. Significant precipitation echoes (> 40 dBZ) have also been frequently detected above 10 km in these two regions by the TRMM Precipitation Radar (PR, Zipser et al. 2006]. Storm distributions have also been examined over the Australia region using simple IR BT thresholding, BT comparisons with reanalysis tropopause temperature, and multispectral IR BT differences [Pope et al. 2008; Romps and Kuang 2009; Young et al. 2012; Aumann and Ruzmaikin 2013]. Though the storm distributions found in these studies are relatively consistent with those derived from lightning and microwave data, their IR-based approaches typically overestimate the areal extent of overshooting updrafts and hazardous weather conditions [Bedka et al. 2010; Bedka et al. 2012].

In summary, climatologies of hazardous storms across the Australia region are sourced from a variety of direct ground- and space-based observations using records that span up to 22 years in duration to derive reliable data over large spatial areas. Though these diverse data records have proven to be extremely valuable, all observing systems except for the World Wide Lightning Network [Virts et al. 2013] have some deficiencies in that they either provide only a few observations per day, have limited spatial coverage, or do not have the range to sample storms over both land and ocean. The TRMM satellite observes the Earth between 35° N and S via a low-inclination orbit, enabling ~4000 observations at any point near the equator and ~13000 observations in the subtropics during the 16-year TRMM LIS period described by Cecil et al. [2015]. The limited swath width of instruments like LIS (600 km) and especially the PR (215 km) coupled with the TRMM precessing orbit does not often permit repeated observations of the same storm system throughout its lifetime. Frequent observations paired with an approach that can pinpoint the locations of intense updrafts are shown to be essential for characterizing the extent and duration of severe hail events from a satellite perspective [Punge et al. 2014]. In contrast, over a 10+ year period extending from July 2005 to December 2015, the Multifunction Transport Satellite (MTSAT) Japanese Advanced Meteorological Imager (JAMI) has observed Australia ~120,000 times at a spatial resolution comparable to that of the TRMM LIS.

This paper describes a 10-year database of OT detections derived from a combination of MTSAT JAMI observations and reanalysis data. As noted above, though OTs detections are not a direct measure of a particular storm-related hazard such as lightning or hail, satellite-observed OT signatures denote strong updraft regions and can serve as a proxy for where weather hazards are occurring. The JAMI instrument collects observations at up to a 15-minute frequency and ~4 km resolution over much of Australia, a combination that exceeds the characteristics of other long-term space-borne datasets. This

OT database provides a unique perspective on the diurnal evolution of hazardous storms with high spatial detail that complements previous analyses.

Data and Methodology

The JAMI instrument was flown aboard the MTSAT-1R and MTSAT-2 satellites. MTSAT-1R was centered at 140° East and was considered to be the operational satellite for meteorological imaging from 28 June 2005 to 30 June 2010. MTSAT-2 was centered at 145° East and served as the operational imager until 4 December 2015. The MTSAT-1R was activated for short time periods during MTSAT-2 maintenance or other temporary technical issues. The time period considered in this study extends 10 years, from 1 July 2005 to 30 June 2015, encompassing almost the full operational lifetime of the MTSAT satellites. The Australia study domain (see Fig. 1) is observed hourly by JAMI with scans beginning approximately 30-minutes after the hour. During the 00, 06, 12, and 18 UTC hours, the region is scanned three times at approximately 15-min intervals which, when combined with the hourly scans, provides a total of 32 images per day. The JAMI pixel size is 4 km at nadir and ~5.5 km along the southern edge of the domain. The 5° eastward shift in nadir position between MTSAT-1R and MTSAT-2 causes the pixel size along the southern edge to increase by ~0.3 km. JAMI observations were acquired from the University of Wisconsin-Madison Space Science and Engineering Data Center (UW-SSEC) via the Man computer Interactive Data Access System (McIDAS-X, Lazzara et al. 1999].

B2010 describes the OT detection algorithm in full detail, but a short summary is provided here for context. The algorithm is formulated around the premise that OTs appear as small clusters of pixels (≤ 15 km diameter) that are significantly colder than the surrounding anvil cloud. Relative BT minima that are ≤ 215 K are first identified. These pixels are then compared to tropopause temperature reanalysis fields to verify that the pixels are indeed cloud tops “overshooting” through the tropopause region. The NASA Modern Era Retrospective analysis for Research and Applications (MERRA, Rienecker et al. 2011] served as the tropopause temperature analysis for this study. The mean BT of the anvil cloud surrounding a tropopause-penetrating pixel is then computed and a pixel is classified as an OT if it is ≥ 6.5 K colder than the anvil mean. Surrounding pixels that belong to the same OT region are then identified if any are present, producing OT regions that cover an area ranging from 1 to 16 pixels. The mean OT extent across the 10-year database is ~6 pixels. Studies have shown that the probability of OT detection ranges from 35-57% based on OT "truth" defined by human OT identifications in MODIS imagery and CloudSat Cloud Profiling Radar data [Bedka et al. 2012; Bedka and Khlopenkov 2016]. The false detection rate ranges from 16-25% based on results from these two studies in addition to comparisons of OT detections with a ground-based radar reflectivity value characteristic of deep convection (≥ 30 dBZ, Dworak et al. 2012]. Bedka and Khlopenkov [2016] discuss some of the challenges associated with IR-based OT detection which provides context for these accuracy statistics.

All available JAMI images throughout the 10-year period were processed by the B2010 OT detection algorithm. The OT detection pixel database was assigned to a 0.25° latitude/longitude grid and the pixel counts per grid box were divided by 10, yielding the mean number of OT pixels per year. OT detection locations were shifted to account for parallax using the OT cloud height assignment method described by Griffin et al. [2016] in combination with MERRA temperature and height profiles interpolated in time to the JAMI image. The image timestamp was adjusted to account for the ~15-minute differential between the timestamp (i.e. the time the first scanline was observed in polar regions of the Northern Hemisphere) and the actual time the center latitude of Australia was scanned. OT detection times were converted to a local solar time (LST) by dividing the longitude by 15° and then adding this time offset to the adjusted JAMI UTC timestamp. Only hourly OT detections were used to characterize the diurnal evolution of OT activity over land and ocean regions and at individual locations of interest throughout the domain (see red labels on Figure 1). Every image was examined by a human analyst to identify noise or other artifacts that could induce errant detections, and OT detections generated from problematic images were omitted from the analysis. Gridded OT detection maps are related to land surface elevation depicted by the one-minute (~2 km) resolution Earth-topographic (ETOPO1) dataset shown in Figure 1.

Results

A map of the total number of OT detections across the 10-year analysis period shows that intense convective storms were most frequent along the northern edge of the NT, the Kimberley Coast, and the western coast of the Cape York Peninsula, with an average of over 200 OT satellite pixels/year over each of these regions (Fig 2a). OT frequencies of greater than 100 pixels/year are quite common over land and ocean north of 20° S latitude A regional OT maximum (up to ~40 pixels/year) is also present along the southeastern coast of the continent and offshore waters and along the northwestern coast of WA. Another local OT maximum (~20 pixels/year) is located over the Indian Ocean south of 40° S latitude.

An analysis of the diurnal distribution of OT detections shows an OT maximum over land in the 16-17 LST timeframe and a broader oceanic maximum peaking at 4-5 LST (Fig. 3a). This timing and overall shape of these peaks matches quite well with previous studies that analyzed differences in the diurnal distribution of precipitation over land and ocean [Nesbitt and Zipser 2003]. The land curve shows an OT increase beginning at 11 LST and dissipating after 22 LST. Thus, we define the 11-22 LST timeframe as "day" and because the storms present during this period formed during the daylight hours with some of these storms persisting into the late evening. The remaining 12 hours are considered "night". Diurnal analyses of OT frequency at individual locations (Fig 3b) show that all major cities except Cairns have a 16-17 LST peak. The Timor Sea, Gulf of Carpentaria, and Indian Ocean regions clearly show peaks during the middle of night. The Indian Ocean OT peak and minimum precede the other two oceanic sites by ~4 hours reflecting the cooler troposphere, and reduced inhibition associated with nocturnal intensification of extratropical cyclones. Regional variations of up to 5 hours in the timing of peak lightning flash density have also been noted by Lay et al. [2007], so thus some variability in results are not unexpected.

Maps of OT detections during day and night and the fraction of OT detections occurring during day (Figs 2b-d) show very clearly the enhancement in storm activity over ocean and reduced storm frequency over or downstream of elevated topography at night. ~70% of OTs were present over land during day and a comparable fraction of OTs were present over ocean at night (Figs 2b and 3a). The high spatial resolution of the OT detection grid depicts the sharp gradient in nighttime activity along coastlines, approaching 100 pixels/year over a 150 km distance in the most extreme case over the northeastern corner of the NT. A close examination of the night OT detection map (Fig 3d) shows two other regions of distinct OT minima over the eastern half of the Cape York Peninsula and inland from the Kimberley Coast. These three regions are co-located with local land elevation maxima (up to ~500 m, Fig. 1) that have cooler and drier nocturnal boundary layers, making the environment unfavorable for nocturnal storm formation. In contrast, at lower elevations nearby along the coast and inland, OT-producing storms can frequently occur (50 pixels/year) at night. Storm activity is also clearly enhanced during at night over the ocean east of New South Wales (NSW) and southeastern QLD associated with organized storms initiated over land that move out to sea, or initiation via low development or trough passage associated with the cooling mid-troposphere during the nocturnal hours. In the winter months (Fig 4) the presence of East Coast Lows also contributes to this signal, typically producing intense convection during their development [Chambers et al. 2014]. A similar difference can be seen on the southern edge of the domain in the Indian Ocean, likely associated with convection associated with the typical track of intensifying extratropical cyclones [Hoskins and Hodges 2005; Allen et al. 2010].

During day, OT-producing storms were most common along elevation gradients and coastal regions of the continent. A sea-breeze circulation producing enhanced moisture convergence causes the local maximum in daytime OT activity over the northwestern coast of WA. The key terrain feature over the southeast of the continent associated with OT-producing storms is the Great Dividing Range, which stretches from BRI-SYD-MLB, providing a localized source of initiation. Storms also often occur (25 pixels/year) during day along the southeastern coast at elevations typically below 100 m, often moving from their initiation points downstream or over higher terrain. One notable exception is the daytime OT maximum in the eastern region of WA where elevations of ~500 m are common. This region was also identified as a local thunder-day and lightning maximum by Kuleshov [2012], and is known to be associated with a locally high number of hail and tornado producing storms [Allen and Karoly 2014, Allen and Allen 2016].

The distribution of OT detections over land agrees quite well with the thunder-day map and the lightning climatologies of Kuleshov [2012] and Cecil et al. [2015], but the agreement between OT and lightning frequency over tropical ocean is rather poor. Williams et al. [2000] indicated that the number of thunderstorms rather than the mean flash rate per storm dominates the large land–ocean lightning difference. Our result shows a comparable number of detections over ocean and nearby land regions, so the number of storms does not explain the lightning difference. A more likely explanation has been proposed by Williams et al [1992] and Zipser and Lutz [1994] who suggested that vertical velocities in oceanic cumulonimbus clouds tend to be lower than those over land. As a result of these weaker updrafts, supercooled liquid water, large ice particles, and ice-ice collisions may not be present in the mixed-phase region in sufficient concentrations to produce storm electrification in many oceanic storms [Zipser and Lutz 1994].

A parameter generated by the B2010 algorithm, the OT-anvil mean BT difference (BTD), can be used as a proxy for updraft strength that will allow us to investigate differences between land and oceanic storms. A greater BTD indicates an OT that has penetrated higher above the surrounding anvil than an OT with a lesser BTD. Griffin et al. [2016] found that an OT cools at an average rate of 7.3 K km^{-1} as it ascends above the anvil based on comparison of B2010 MODIS BTD data with CloudSat radar profiles. GOES Imager and MTSAT JAMI data is four times coarser spatially than MODIS, causing these GEO instruments to record BTDs that are 2.4-3.9 K less than MODIS (see Equations 4-5 from Griffin et al. 2016]. We examine all OTs detected within the 10-20° S and 122-147° E domain where the number of overall OT detections and ambient storm environment are comparable for land and ocean regions. We find that the mean BTD over land (ocean) is -11.05 K (-10.43 K), indicating that the average OT over land penetrates 0.13-0.18 km higher above the anvil than an OT over ocean. The interquartile range over land (ocean) is -7 to -12.8 K (-6.9 to 12.2 K), which implies that fewer storms with extreme updrafts are present during night. These results provide further evidence that oceanic storms do have weaker updrafts near cloud top that likely signify dynamical and microphysical differences and reduced storm electrification deeper within the cloud as noted in previous studies.

Monthly analyses of OT detection output show differences in the distribution of convection throughout the year (Fig 4). OTs are almost never found over the northern third of continental land from May-September, reflecting the dry season. Storms then begin to develop in October over the NT and are significantly more frequent over land relative to offshore ocean from October-November, prior to the summer monsoonal period. OT activity peaks in this region over both land and ocean in January associated with the monsoon period. Storms with OTs can occur in almost any month of the year except for August and September in the southeastern portion of the domain. Activity peaks over land here in the November-December timeframe, reflecting the peak season of both ordinary convection [Dowdy et al. 2014] and severe convection [Allen and Karoly 2014]. Storms can occur throughout much of the year over ocean, aided by the warm water transported southward by the East Australian Current and periodic extratropical disturbances such as transitioning extratropical cyclones or East Coast Lows [Chambers et al. 2014].

Over the Indian Ocean along the southern edge of the domain, OT activity peaks during the winter months of June-August. This time period coincides with the presence of frequent mid-latitude cyclones and frontal systems that tend to produce convection more often during the night-time hours based on Fig. 3b [Allen et al. 2010]. Personal experience of the author and studies such as Proud [2014] show that the B2010 algorithm can also produce false detection in scenes with cold cirrus oriented in complex patterns that can "look like" OT regions from a computer algorithm perspective. While this may be occurring to some extent over this Indian Ocean region, the facts that 1) OT detections are most frequent here during night similar to other confirmed areas of oceanic storm activity and 2) Virts et al. [2013] show an area of enhanced lightning frequency in this region and 3) the area is associated with a local maxima in the storm track and explosive cyclogenesis that often produces deep convection [Hoskins and Hodges 2005, Allen et al. 2010] that suggests that the detections found over this region are reasonable.

Summary

This paper describes a 10-year OT detection database over Australia derived from a combination of MTSAT JAMI IR observations and NASA MERRA reanalysis data. The results show OT distributions over land that generally agree with previous approaches for evaluating land-based hazardous storm activity. A distinct diurnal variation in OT activity between land and ocean was present, with ∼70% of storms occurring over land during day and a comparable percentage occurring over ocean at night. The high spatial resolution analyses enabled by the relatively frequent sampling of the JAMI showed interesting details such as the impact of land surface elevation and elevation gradients on OT-producing storm activity. OTs were detected more frequently over ocean at night than would be inferred from storm distributions based on previous TRMM, OTD, and WWLN lightning detection analyses. Updrafts near cloud top were found to be slightly stronger in land-based storms over the tropics than nearby storms over ocean based on differences in magnitude of OT penetration above the surrounding anvil. We assume that updrafts within land-based storms are also stronger at lower altitudes within the mixed-phase region where charge separation and electrification typically occurs, consistent with findings from previous studies that have examined land-ocean lightning differences.

The spatial and temporal detail provided by long-term GEO-based OT detection databases has proven to be quite useful in several studies for understanding the distribution of hazardous storms over regions without a long-term, climate-quality, and spatially contiguous ground-based radar or lightning detection networks. Recent advances in OT detection capability [Bedka and Khlopenkov 2016] coupled with more frequent and detailed data provided by the next generation of GEO imagers such as the GOES-R Advanced Baseline Imager [Schmit et al. 2005] and the Japanese Advanced Himawari Imager [Bessho et al. 2016] will only serve to improve the quality of future OT detection analyses for weather and climate applications. Over the Australian region these satellite-based datasets will provide critical real-time assessment of hazardous thunderstorms in the coming decades, along with complementary climatologies [Allen and Allen 2016]. GEO-based OT detections will also provide a valuable complement to the more frequent but spatially coarser space-based lightning detection observations provided by instruments such as the GOES-R Geostationary Lightning Mapper [Goodman et al. 2013].

Acknowledgements

Generation of the MTSAT JAMI Australia region OT database was funded by Willis Limited via the NASA Space Act Agreement (UK-0533-0). JTA acknowledges support from the U.S. Office of Naval Research (N00014-12-1-0911). The MTSAT JAMI OT detection database is available for research use upon request from the authors.

References

Allen, J. and D. Karoly (2014), A Climatology of Australian Severe Thunderstorm Environments 1979-2011: Inter-annual Variability and the ENSO Influence. *Int. Jour. Climatol.,* **34**, 81–97. DOI: 10.1002/joc.3667

Allen, J. T. and E. R. Allen (2016), A review of severe thunderstorms in Australia. *Atmos. Res.*, **178-179**, 347-366. doi: 10.1016/j.atmosres.2016.03.011.

Allen, J. T., D. Karoly, and G. A. Mills (2011), A severe thunderstorm climatology for Australia and associated thunderstorm environments. *Aust. Meteor. Oceanogr. Jour.*, **61**, 143-158.

Allen, J. T., A. B. Pezza, and M. T. Black (2010), Explosive cyclogenesis: A global climatology comparing multiple reanalyses. *J. Climate*, ***23***, 6468–6484. doi: 10.1175/2010JCLI3437.1

Aumann, H. H., and A. Ruzmaikin (2013), Frequency of deep convective clouds in the tropical zone from 10 years of AIRS data. *Atmos. Chem. Phys.*, **13**, 10795–10806

Bedka, K. M., J. Brunner, R. Dworak, W. Feltz, J. Otkin, and T. Greenwald (2010), Objective satellite-based overshooting top detection using infrared window channel brightness temperature gradients. *J. Appl. Meteor. And Climatol.*, **49**, 181-202.

Bedka, K. M. (2011), Overshooting cloud top detections using MSG SEVIRI infrared brightness temperatures and their relationship to severe weather over Europe. *Atmos. Res.*, **99**, 175-189.

Bedka, K. M., R. Dworak, J. Brunner, and W. Feltz (2012), Validation of satellite-based objective overshooting cloud top detection methods using CloudSat Cloud Profiling Radar observations. *J. Appl. Meteor. And Climatol.,* **27**, 684-699.

Bedka, K. M., C. Wang, R. Rogers, L. Carey, W. Feltz, and J. Kanak (2015), Examining deep convective cloud evolution using total lightning, WSR-88D, and GOES-14 Super Rapid Scan datasets**.** *Wea. Forecasting,* **30,** 571-590

Bedka, K. M., and K. Khlopenkov (2016), A probabilistic multispectral pattern recognition method for detection of overshooting cloud tops using passive satellite imager observations. *J. Appl. Meteor. And Climatol.* In Press.

Bessho, K., and co-authors (2016), An introduction to Himawari-8/9 - Japan's new generation geostationary meteorological satellites. J. Meteorological Society of Japan, In Press.

Cecil, D. J., and C. B. Blankenship (2012), Toward a global climatology of severe hailstorms as estimated by satellite passive microwave imagers. *J. Climate*, **25**, 687–703, doi:10.1175/JCLI-D-11-00130.1

Cecil, D. J., D. E. Buechler, R. J. Blakeslee (2014), Gridded lightning climatology from TRMM-LIS and OTD: Dataset description. *Atmos. Res*., **135-136**, 404-414.

Cecil, D. J., D. E. Buechler, and R. J. Blakeslee (2015), TRMM LIS Climatology of Thunderstorm Occurrence and Conditional Lightning Flash Rates. *J. Climate*, **28**, 6536–6547. doi: http://dx.doi.org/10.1175/JCLI-D-15-0124.1

Chambers, C. R. S., G. B. Brassington, K. Walsh and I. Simmonds (2015), Sensitivity of the distribution of thunderstorms to sea surface temperatures in four Australian east coast lows. *Meteor. Atmos. Phys.,* **127**, 499-517.

Dowdy, A. J., and Kuleshov, Y. (2014), Climatology of lightning activity in Australia: spatial and seasonal variability. *Aust. Meteor. Oceanogr. Jour.,* **6**, 9-14.

Dworak, R., K. M. Bedka, J. Brunner, and W. Feltz (2012), Comparison between GOES-12 overshooting top detections, WSR-88D radar reflectivity, and severe storm reports. *Wea. Forecasting*. **10**, 1811-1822

Ferraro, R., Beauchamp J., Cecil D., Heymsfield G. (2014), A prototype hail detection algorithm and hail climatology developed with the advanced microwave sounding unit (AMSU), *Atmos. Res.*, http://dx.doi.org/10.1016/j.atmosres.2014.08.010

Goodman, S. J., R. J. Blakeslee, W. J. Koshak, D. Mach, J. Bailey, D. Buechler, L. Carey, C. Schultz, M. Bateman, E. McCaul, and G. Stano (2013), The GOES-R Geostationary Lightning Mapper (GLM). *Atmos. Res.* **125-126**, 34-49.

Griffin, S., K. Bedka, and C. Velden (2016), A method for calculating the height of overshooting convective cloud tops using satellite-based IR imager and CloudSat Cloud Profiling Radar observations. *J. Appl. Meteor. Climatol*. **55**, 479-491. doi:10.1175/JAMC-D-15-0170.1

Hoskins, B. J. and K. I. Hodges (2005), A New Perspective on Southern Hemisphere Storm Tracks. *J. Climate*, **18**, 4108-4129.

Kuleshov, Y. (2012), *Thunderstorm and Lightning Climatology of Australia*, Modern Climatology, Dr Shih-Yu Wang (Ed.), ISBN: 978-953-51-0095-9, InTech, Available from:

http://www.intechopen.com/books/modern-climatology/thunderstorm-and-lightning-climatology-of-australia

Lay, E. H., A. R. Jacobson, R. H. Holzworth, C. J. Rodger, and R. L. Dowden (2007), Local time variation in land/ocean lightning flash density as measured by the World Wide Lightning Location Network, *J. Geophys. Res.*, **112**, D13111, doi:10.1029/2006JD007944.

Lazzara, M. A., and co-authors (1999), The Man Computer Interactive Data Access System: 25 years of interactive processing. *Bull. Amer. Meteor. Soc.*, **80**, 271–284.

Pope, M., C. Jakob, and M. J. Reeder (2008), Convective systems of the north Australian monsoon. *J. Climate*, **21**, 5091–5112, doi:10.1175/2008JCLI2304.1.

Proud, S. R. (2014), Analysis of overshooting top detections by Meteosat Second Generation: a 5-year dataset. *QJRMS*, DOI: 10.1002/qj.2410

Punge, H. J., K. M. Bedka, M. Kunz, A. Werner (2014), A new physically based stochastic event catalog for hail in Europe*. Natural Hazards,* **73**, 1625-1645.

Rienecker, M. et al. (2011), MERRA: NASA's Modern-Era Retrospective Analysis for Research and Applications. *J. Climate*, **24**, 3624–3648. DOI: 10.1175/JCLI-D-11-00015.1

Romps, D. M., and Z. Kuang (2009), Overshooting convection in tropical cyclones, *Geophys. Res. Lett.*, **36**, L09804, doi:10.1029/2009GL037396.

Schmit, T. J., M. M. Gunshor, W. P. Menzel, J. Li, S. Bachmeier, and J. J. Gurka (2005), Introducing the next-generation Advanced Baseline Imager (ABI) on GOES-R. Bull. Amer. Meteor. Soc., 86, 1079–1096, doi:10.1175/BAMS-86-8-1079

Thiery, W., E. L. Davin, S. I. Seneviratne, K. M. Bedka, S. Lhermitte, N. van Lipzig (2016), Lake Victoria, a hotspot of future hazardous thunderstorm intensification. Submitted to *Nature Communications.*

Virts, K. S., J. M. Wallace, M. L. Hutchins, and R. H. Holzworth (2015), Diurnal and seasonal lightning variability over the Gulf Stream and Gulf of Mexico. *J. Atmos. Sci.*, **72**, 2657–2665, doi:10.1175/JAS-D-14-0233.1

Williams ER, Rutledge SA, Geotis SG, Renno N, Rasmussen,E, Rickenbach T (1992), A radar and electrical study of tropical “hot towers”. *J Atmos Sci*, 49, 1386-1395

Williams, E., K. Rothkin, D. Stevenson, and D. Boccippio (2000), Global Lightning Variations Caused by Changes in Thunderstorm Flash Rate and by Changes in the Number of Thunderstorms. *J. Appl. Meteor.*, **39**, 2223–2230. doi: http://dx.doi.org/10.1175/1520-0450(2001)040<2223:GLVCBC>2.0.CO;2

Young, A. H., J. J. Bates, and J. A. Curry (2012), Complementary use of passive and active remote sensing for detection of penetrating convection from CloudSat, CALIPSO, and Aqua MODIS, *J. Geophys. Res.,* 117, D13205, doi:10.1029/2011JD016749.

Zipser, E. J., and K. R. Lutz (1994), The vertical profile of radar reflectivity of convective cells: A strong indicator of storm intensity and lightning probability?, *Mon. Wea. Rev.*, 122, 1751–1759.

Zipser, E. J., J. C. Daniel, C. Liu, S. W. Nesbitt, and D. P. Yorty (2006), Where are the most intense thunderstorms on Earth?, *Bull. Am. Meteorol. Soc.*, 87, 1057 – 1071.

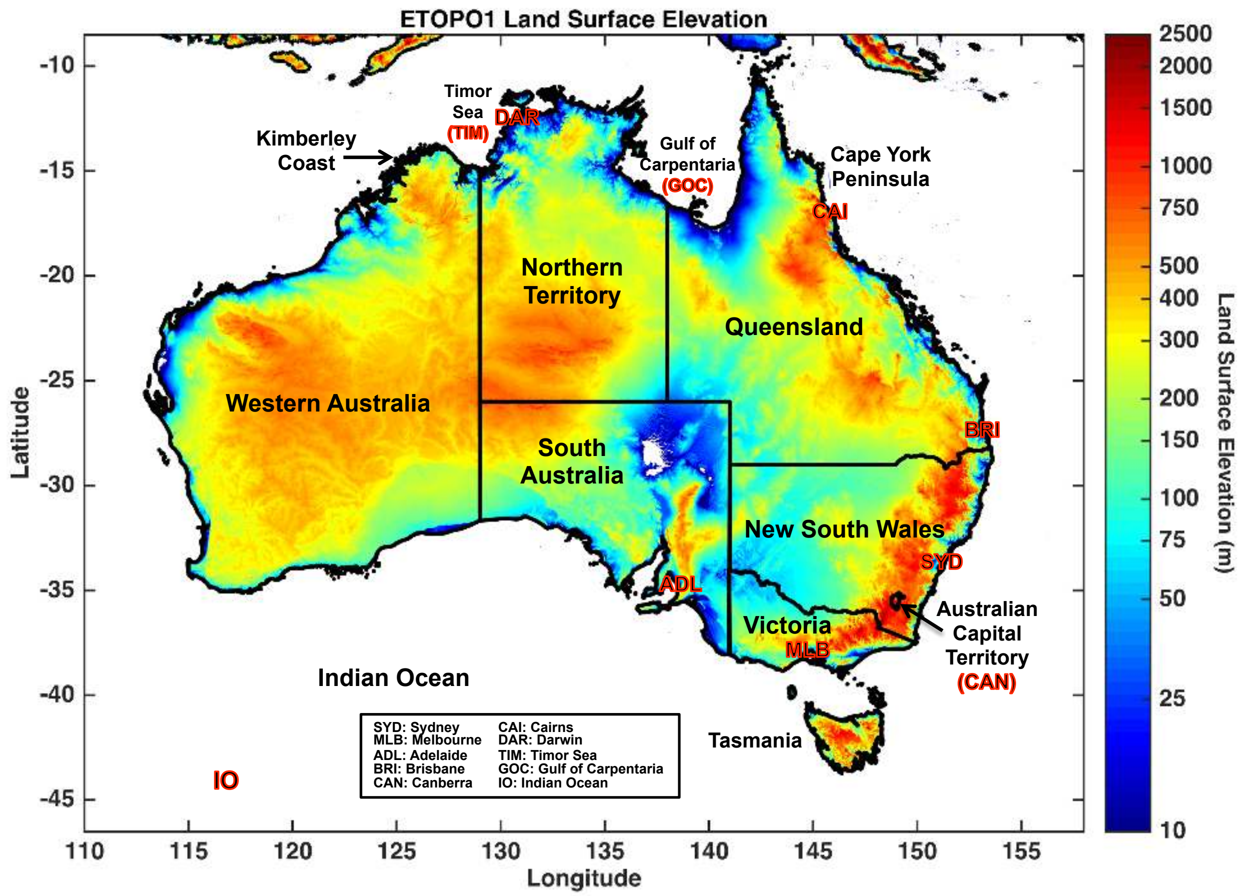

Figure 1: Land surface elevation over Australia (in meters) from the ETOPO1 dataset. Australian states and territory boundaries are overlaid in addition to locations of cities and regions discussed in the text.

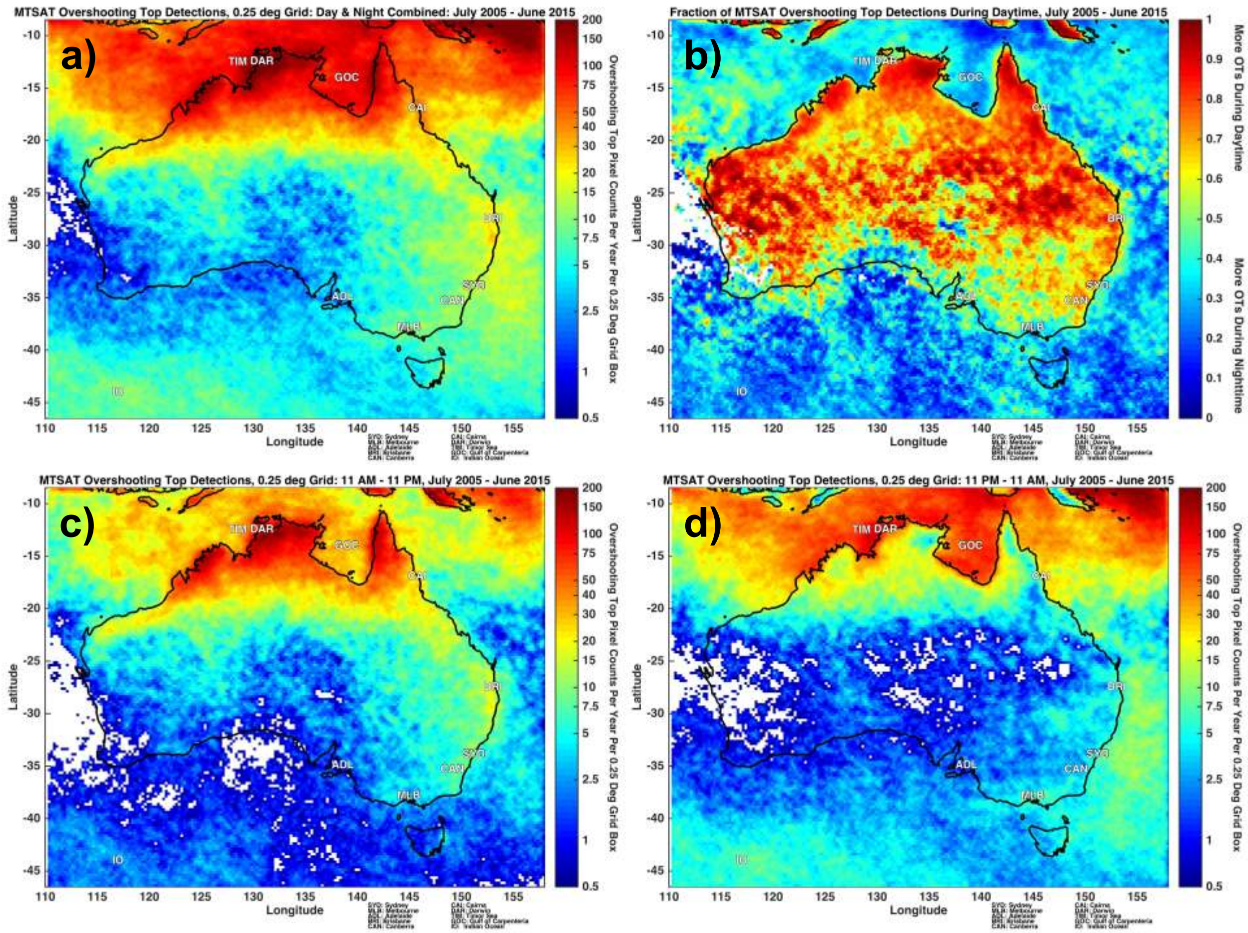

Figure 2: a) A map of the mean number of OT pixel detections per year within each 0.25° grid box using all available MTSAT JAMI scans. b) The fraction of daily OT detections occurring during each hour over Australia (red line) and ocean (blue line) using the hourly OT detection dataset. c) A map of the mean number of OT detections per year within each 0.25° grid box from 1100 AM - 1059 PM solar time. d) Same as c) but for 1100 PM - 1059 AM solar time.

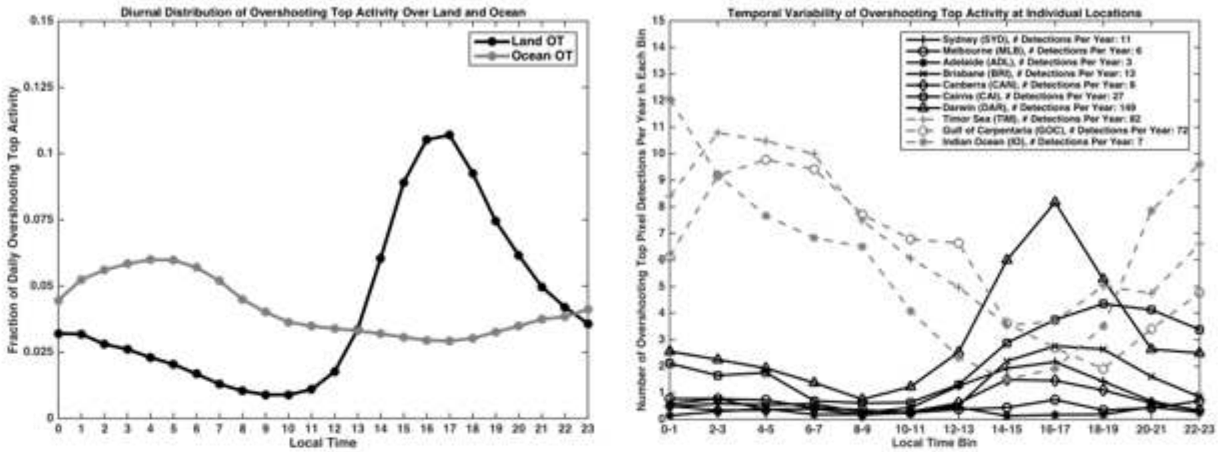

Figure 3: a) The fraction of daily OT pixel detections occurring during each hour over Australia (black line) and ocean (grey line) using the hourly OT detection dataset. b) The mean number of OT pixel detections per year occurring within two-hour bins at 10 individual sites identified in Figure 1. Sites over land (ocean) are colored in black (grey). The Darwin site data has been scaled by a factor of 4 to fit within the range of the other sites.

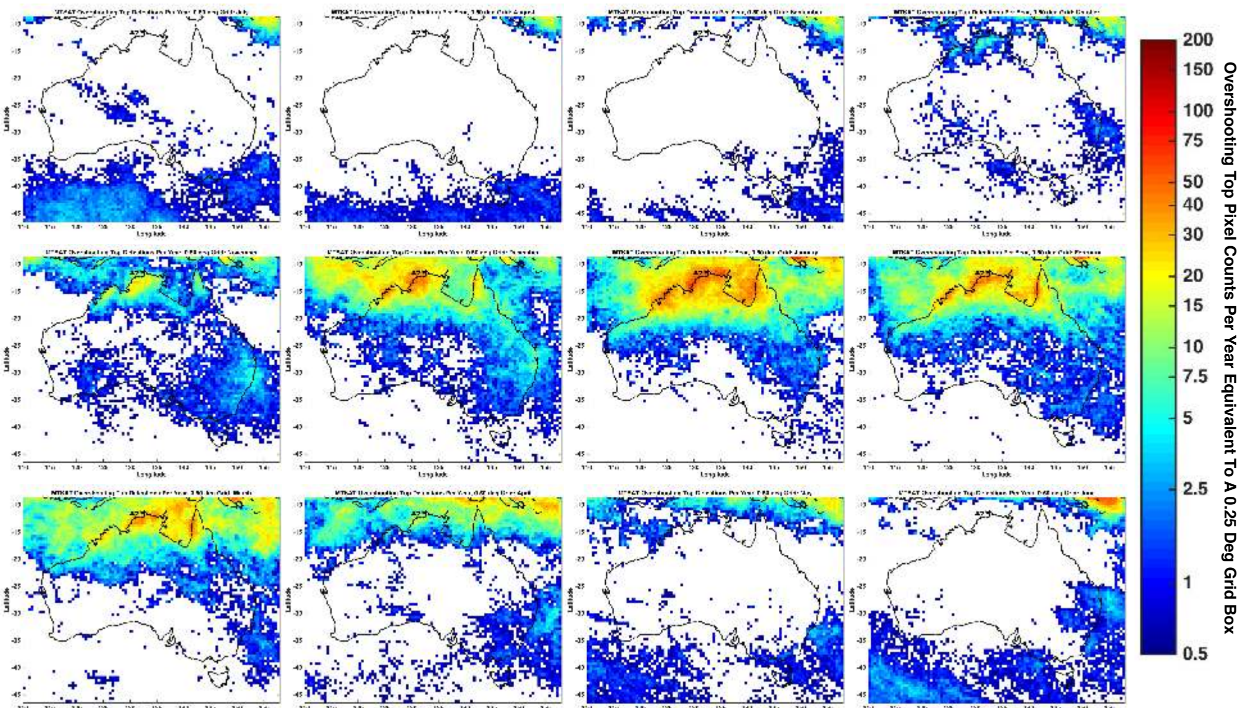

Figure 4: Maps of OT pixel detection counts per year within each 0.50° grid box during each month of year. Top row: July-October, middle row: November-February, bottom row: March-June. Counts are divided by four to make the values and color table equivalent to the 0.25° resolution analyses shown in Figure 2.